Appl. Phys. A (2017)123:652
DOI 10.1007/s00339-017-1252-3

Applied Physics A
Materials Science & Processing

Comparison of jets from Newtonian and non-Newtonian fluids induced by blister-actuated laser-induced forward transfer (BA-LIFT)

Emre Turkoz[1] · Luc Deike[1,2] · Craig B. Arnold[1]

Received: 27 June 2017 / Accepted: 8 September 2017

Abstract Blister-actuated laser-induced forward transfer (BA-LIFT) is a high-resolution printing technique, where small droplets are ejected from a thin liquid layer onto a receiver substrate. Experiments with a high-speed camera imaging setup demonstrate novel regimes during the jet formation for the transfer of viscoelastic shear-thinning polymer solutions compared to Newtonian fluids. The ratio of the ink film thickness H_f to the blister height H_b is used as a dimensionless number H_f/H_b to classify different jet behaviors. We show that different H_f/H_b thresholds can be defined depending on the elasticity of the ink layer for the induced jets to result in breakup.

1 Introduction

Laser-induced forward transfer (LIFT) is a nozzle-less printing technique [1] that has been developed over the years to print various types of materials including polymers [2], biomaterials [3], conducting silver pastes [4], thin metal films [5], carbon nanotubes [6], and viscoelastic alginate solutions [7]. Blister-actuated laser-induced forward transfer (BA-LIFT) is a variation of LIFT where there is an interfacial polymer layer between the transparent substrate and the ink layer [8]. This technique has been developed to prevent possible disruptions in mechanical and chemical integrity due to laser–ink interactions, and proven to be successful in transferring sensitive materials [9]. The physics of blister formation for this process has been investigated experimentally [10] and numerically [11], and it has been shown that a 355 nm wavelength laser pulse (20 ns) with a Gaussian beam profile focused on a polyimide thin layer results in reproducible blisters whose height and radius values are functions of the laser energy. The jet formation from Newtonian fluids has been investigated experimentally using time-resolved imaging [12] and numerically using computational fluid dynamics (CFD) [13]. In addition, an analytical model [14] for the early time dynamics of the BA-LIFT process shows that the fluid around the blister undergoes shear as the ink at the vicinity of the blister is pulled towards the center of the blister during jet formation.

While BA-LIFT studies so far have focused on the evaluation of the underlying physics with jets created using Newtonian fluids, real-life applications require the adaptation of this technique to various types of materials that exhibit complex rheological properties [15, 16]. In this study, we present the features of jets induced using viscoelastic inks with the BA-LIFT technique. Compared to the jets created from Newtonian fluids, the jets from viscoelastic inks exhibit a very high stretchability due to their elasticity, which competes with the surface tension-driven thinning [17]. We report that there exists a critical jet velocity that would result in the breakup of jets.

2 Experimental methods

Different concentrations of xanthan gum (XG) in water are used as model non-Newtonian solutions. XG solution is selected as the rheological modifies because of the extensive literature dedicated to studying these solutions, its

✉ Craig B. Arnold
cbarnold@princeton.edu

[1] Department of Mechanical and Aerospace Engineering, Princeton University, Princeton, NJ, USA

[2] Princeton Environmental Institute, Princeton University, Princeton, NJ, USA

Published online: 19 September 2017

inherent viscoelasticity, and the convenient shear-thinning behavior of its viscosity [18]. We prepare XG in water solutions with four different concentrations ([XG] = 0.05, 0.1, 0.2, and 0.4 wt%). Triton X-100 surfactant (1.0 wt%) is added to the solution to increase the wettability of XG solution on the polyimide. The solutions are stirred for 24 h before the rheological measurements and BA-LIFT experiments to ensure homogeneity.

The model Newtonian fluid used in this study is *N*-methyl-2-pyrrolidone (NMP) with the viscosity $\mu = 1.7$ mPa s, the density $\rho = 1030$ kg/m^3, and the surface tension $\gamma = 40.79$ mN/m.

The shear rheometry of solutions is evaluated using Anton Paar Physica MCR-301 rheometer using a double-gap geometry. Small amplitude oscillatory shear rheometry in linear viscoelastic regime is utilized to evaluate the yield stress of the solutions.

The interfacial polyimide layer is prepared by spin coating polyimide resin (HD Microsystems PI2525) onto glass microscope slides at 500 rpm for 10 s followed by a faster spin at 3000 rpm for 40 s. Subsequently, the slides are baked at 120 °C for 30 min followed by another 30 min at 360 °C to complete the imidization process, which yields 6.9 µm-thick polyimide layers on glass slides. The inks are coated on the polymer layer using a blade coater. The thin-film thicknesses are measured using a confocal microscope.

A frequency-tripled Nd:YVO_4 laser (Coherent AVIA, 20 ns) is used to generate a pulse with 355-nm wavelength [10]. The laser beam diameter is approximately 20 µm. High-speed videos are captured using a Phantom v2512 (Vision Research) camera with a range of 500,000–700,000 frames per seconds and 0.26 px/µm resolution thanks to a 10× objective (Mitutoyo). The camera exposure time is 1.0 µs. Since the high-speed camera works in a post-trigger capture setting with a continuous backlight, the first image where the laser pulse or a jet feature is visible is designated as t_0, which denotes the reference time. With the use of the high speed of the camera, we could obtain multiple images during the jet motion, and analyze the formation of jets from non-Newtonian fluids.

3 Results

3.1 Characterization of inks

XG solutions exhibit shear-thinning and their shear viscosity values can be expressed in the form of a power law $\mu(\dot{\gamma}) = a\dot{\gamma}^n$, where $\dot{\gamma}$ is the shear rate, n is the exponent, and a is the power law coefficient. The shear-thinning exponent decreases and the zero-shear viscosity increases with the XG concentration ([XG]). The yield stress τ_y is evaluated using shear oscillatory rheometry by doing a stress sweep at 1 Hz and reading the cross-over of elastic (G′) and loss (G″) moduli. These values are presented in Table 1 along with the power law parameters for XG solutions used in this study.

Table 1 Coefficients of the power law $\mu(\dot{\gamma}) = a\dot{\gamma}^n$ of viscosity versus shear rate with yield stress τ_y values

[XG] (%)	a	n	τ_y (Pa)
0.05	0.269	−0.607	0.6
0.1	0.365	−0.642	1.4
0.2	1.122	−0.740	2.1
0.4	2.14	−0.772	4.0

The addition of surfactant affects the surface tension of the solutions drastically. Using a pendant drop method, the surface tension of the solutions is evaluated as 30.6 mN/m.

Due to the low concentration of XG, the solutions can be assumed to have the same density as water ($\rho_w = 1000$ kg/m^3). NMP and XG solutions, therefore, have very similar density and surface tension values. Furthermore, since XG solution is water-based and shear-thinning, its viscosity approaches water viscosity ($\mu_w = 1.002$ mPa s) at high shear-rates associated with the BA-LIFT process. The biggest difference between these two inks is the inherent elasticity of the XG solutions.

3.2 Blister profiles

Blisters are generated on the polyimide film using a laser pulse that has a Gaussian-like profile. The absorption process and the resulting blister formation are depicted in Fig. 1a. The laser pulse causes the decomposition of the polyimide layer, which leads to the ablation of polyimide from the transparent glass substrate. While the initial ink layer thickness is denoted with H_f, the radius and the height of the resulting blisters are denoted with R_b and H_b, respectively.

Blister profiles measured using a confocal microscope are plotted in Fig. 1b. Figure 1b shows that the blister height H_b increases with the laser energy. Since the pulse duration is constant from one pulse to the next, larger blister height is an indication of the faster blister expansion. Keeping the beam diameter constant and changing the laser energy between 14.4 and 28.2 µJ, the height of the blister can be assumed to be linearly dependent on the laser energy as $H_b = 0.6684E-0.78$ (in µm), where E is the laser energy. On the other hand, the ink thickness H_f is directly proportional to the resistance due to inertia to the blister expansion. It was shown that the threshold laser energy for material transfer depends on the ink thickness linearly for Newtonian inks [13]. Thus, we define a dimensionless parameter as H_f/H_b to compare the effect of

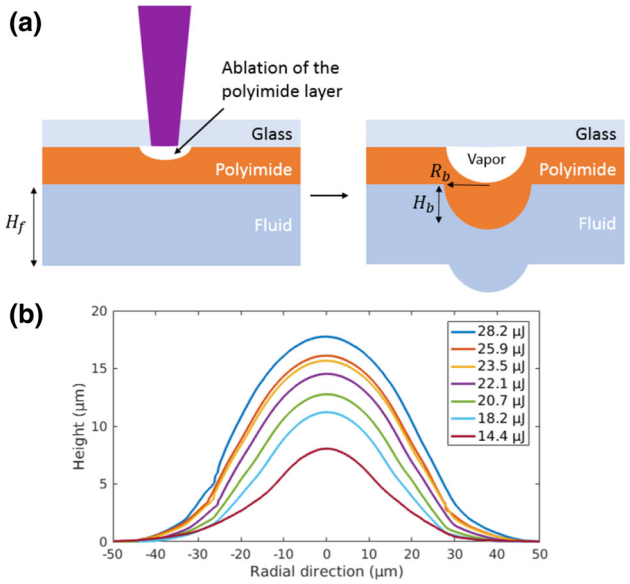

Fig. 1 Absorption of the laser energy by the polyimide layer and the blister generation. **a** Dimensionless parameter H_f/H_b is utilized to denote the relative effect of the blister expansion to the resistance against the jet formation by the bulk fluid. **b** Blister profiles corresponding to different laser energies measured by laser scanning microscopy

the fluid ink thickness to the energy deposited into the system. We note that the H_f/H_b parameter does not include any information about the radius and the shape of the blister, and a more general analysis which includes different blister shapes and radii would require the utilization of a different dimensionless parameter.

3.3 Images of BA-LIFT jets

3.3.1 Comparison of jet images from non-Newtonian and Newtonian fluids

Figure 2a, b shows jets induced from a 57 μm-thick NMP ink, where a high energy blister ($H_b = 16.2$ μm, $H_f/H_b = 3.51$) results in multiple droplet formation (Fig. 2a), and a low energy blister ($H_b = 8.6$ μm, $H_f/H_b = 6.63$) results in jetting without breakup (Fig. 2b). We observe that the jet is faster and stretches more to breakup into multiple droplets than the jetting without breakup case. The jet presented in Fig. 2a reaches 430.4 μm in 1.82 μs, while the jet in Fig. 2b reaches only 52 μm in 14.54 μs.

Multiple-drop breakup and jetting without breakup cases for XG solutions are presented in Fig. 3a, b, respectively. These figures show the multiple-drop breakup and jetting without breakup regimes obtained for [XG] = 0.05 wt%. Both multiple-drop and jetting without breakup regimes are qualitatively very different from these regimes observed with XG solutions. It is seen from Fig. 3a that even if the non-Newtonian filament stretches up to a similar amount as the Newtonian filament in Fig. 2a, the non-Newtonian filament does not pinch-off from the base of the jet as the Newtonian jet does at $t_0 + 27.27$ μs, but instead, the non-Newtonian jet breaks a certain distance away from its base that is larger than its radius. In addition, we do not see the formation of multiple droplets from the long non-Newtonian filament as is the case with the Newtonian filament at

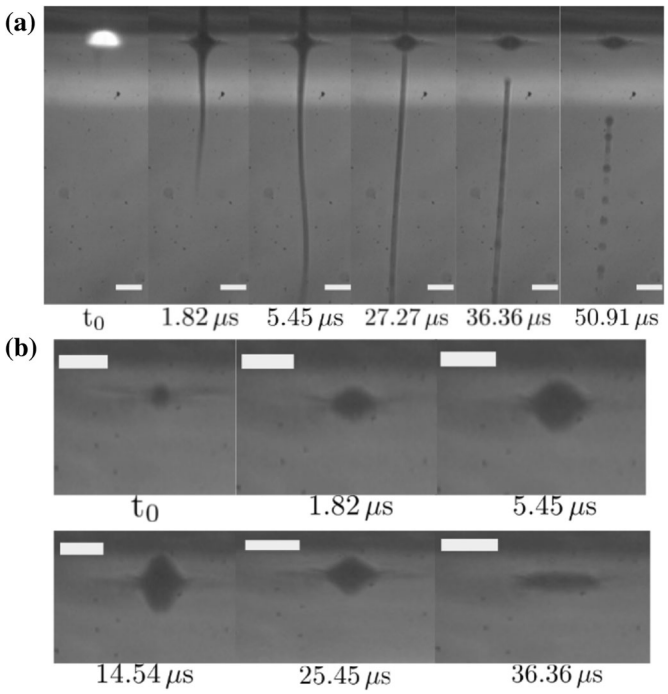

Fig. 2 Two different cases of high-speed imaging with NMP ($H_f = 57$ μm): **a** high energy blister ($H_b = 16.2$ μm, $H_f/H_b = 3.51$) resulting in breakup with multiple drops, **b** low energy blister ($H_b = 8.6$ μm, $H_f/H_b = 6.63$) resulting in jetting without breakup. Images are from the videos captured by the high-speed camera, and t_0 is the reference time. Scale bars represent 75 μm

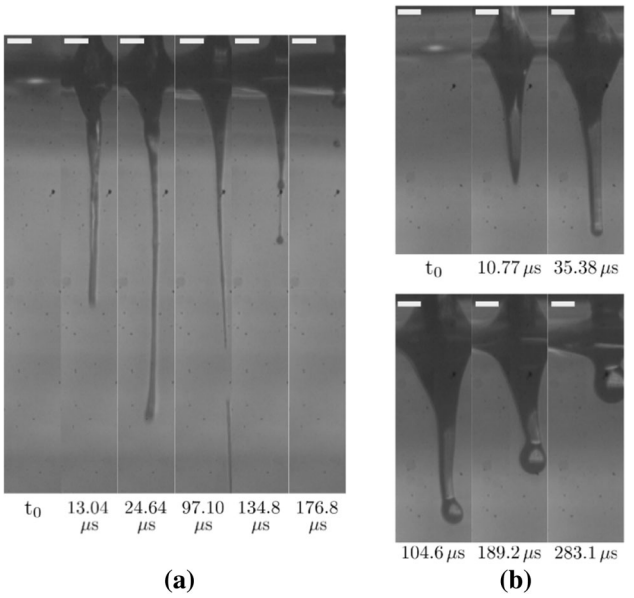

Fig. 3 Two different cases of high-speed imaging with [XG] = 0.05 wt%: **a** high energy blister ($H_b = 16.2$ μm, $H_f/H_b = 6.80$) resulting in breakup with multiple drops, **b** low energy blister ($H_b = 8.6$ μm, $H_f/H_b = 8.65$) resulting in jetting without breakup. Images are from the videos captured by the high-speed camera, and t_0 is the reference time. Scale bars represent 75 μm

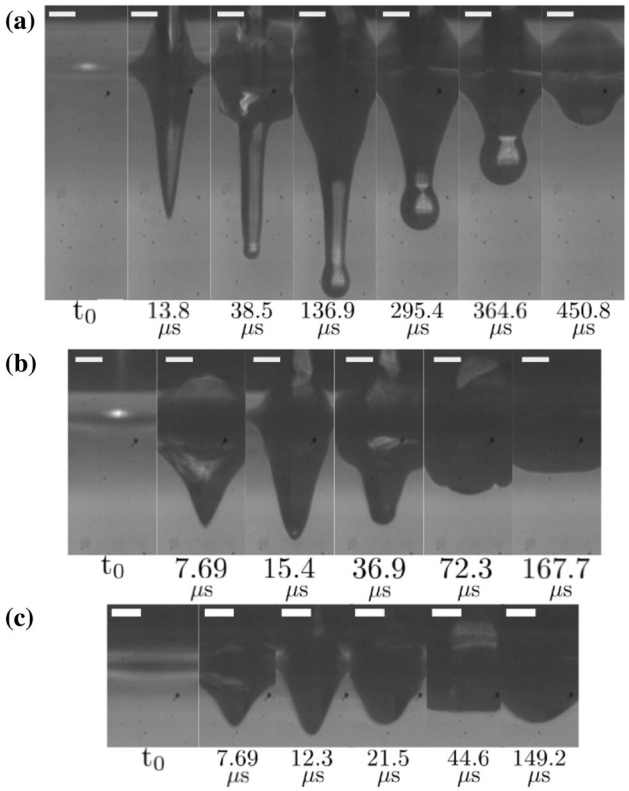

Fig. 4 Different amounts of stretching versus elasticity. Higher elasticity affects the amount of stretching. **a** [XG] = 0.1 wt%, $H_f/H_b = 5.65$. **b** [XG] = 0.2 wt%, $H_f/H_b = 5.06$. **c** [XG] = 0.4 wt%, $H_f/H_b = 5.63$. Images are from the videos captured by the high-speed camera, and t_0 is the reference time. Scale bars represent 75 μm

$t_0 + 50.91$ μs. This comparison shows us that the viscoelasticity reduces the number of droplets produced from a single filament. This matches the observation presented in a work on the fragmentation of viscoelastic filaments [19], where it is shown that fewer droplets are formed from viscoelastic filaments compared to Newtonian filaments. The inherent viscoelasticity of XG inks slows the radial thinning of the jet, which causes fewer droplets compared to a jet formed from NMP inks. We also observe that the droplet is getting larger as the jet is retracted.

Comparing Fig. 2b with Fig. 3b indicates that the features for the jetting without breakup are very different between these two types of fluid. We observe that the non-Newtonian jet created using [XG] = 0.05 wt% solution can be stretched more than the Newtonian jet created using NMP and it still can retract without producing a droplet. The NMP jet in Fig. 2b stretches 91% of the ink film thickness, while the XG jet stretches 549% of the ink film thickness.

3.3.2 *Stretching and elasticity of jets from xanthan gum solutions*

An important feature observed during the experiments is the amount of stretching associated with XG concentrations. We observe that as the yield stress τ_y of the fluid increases, the amount of maximum stretching decreases for similar H_f/H_b values. This is shown in Fig. 4a–c, where images for the jetting without breakup regime for [XG] = 0.1, 0.2, and 0.4 wt% are presented, respectively. It is shown in these figures that for similar H_f/H_b values, the amount of stretching decreases as the polymer concentration increases. In these figures, the jets stretch up to 842, 339, and 243% of their initial ink thickness values for [XG] = 0.1, 0.2, 0.4 wt%, respectively.

We see in Fig. 4a that for [XG] = 0.1 wt% and $H_f/H_b = 5.65$, a droplet is formed at the tip of the jet. This droplet grows as the jet gets retracted to the ink, which indicates that there is a point along the filament where the axial jet velocity is zero.

Figure 4b shows images for the [XG] = 0.2 wt% and $H_f/H_b = 5.06$ case. As the jet retracts back, we see the formation of a shoulder-like structure around 36.9 μs. This structure stays as the jet is retracted, which eventually rounds up and remains visible as long as 167.7 μs.

Figure 4c shows images for the [XG] = 0.4 wt% and $H_f/H_b = 5.63$. We see that the least amount of stretching is observed at this case. This is expected, because [XG] = 0.4 wt% solutions have the highest yield stress ($\tau_y = 4.0$ Pa) among all the solutions used in this study. In this case, we do not see the formation of a shoulder very

clearly; however, the retracted jet rounds up and is still visible at 149.2 μs.

A sample of jet length versus time curves is plotted in Fig. 5. Except for the first two series ($H_f/H_b = 5.14$ and $H_f/H_b = 6.80$ with [XG] = 0.05 wt%), all the data points belong to the cases where jets eventually retract back to the ink layer surface. We note that the two cases with breakup have a distinctively higher velocity compared to the cases without breakup. In addition, we see that the amount of stretching increases as the relative ink thickness H_f/H_b is decreased. From our experiments, we see that the threshold H_f/H_b values for breakup can be listed as given in Table 2. This also suggests that a critical velocity or Weber number ($We = \rho U_{jet}^2 R_{jet}/\sigma$, where ρ is the ink density, U_{jet} is the axial jet velocity, R_{jet} is the jet radius, and σ is the surface tension) might be necessary to obtain drops on viscoelastic ligaments as in the case of Newtonian filaments [20], while this threshold might depend on the yield stress of the viscoelastic filament.

We observe from our experiments that there are two main factors that determine the features of the viscoelastic jets: (1) relative ink thickness compared to the blister height (H_f/H_b); (2) polymer concentration, which affects the yield stress τ_y and viscosity of the ink. The increasing ink thickness results in larger inertial resistance as explained in [13], where the threshold energy for jet formation has been shown to be linearly dependent on the ink thickness for Newtonian inks. In addition to the inertial effects, for our experiments, the elasticity and high viscosity of the ink layer come into the picture. Due to the shear-thinning behavior of the ink layer, the effective viscosity of the ink decreases as the fluid from the vicinity of the blister gets pulled in towards the center of the blister [14]. After jet formation, the liquid filament resists the motion in the axial direction. The resistance is proportional to the elasticity of the filament; therefore, a higher laser energy is required to stretch filaments with higher elasticity.

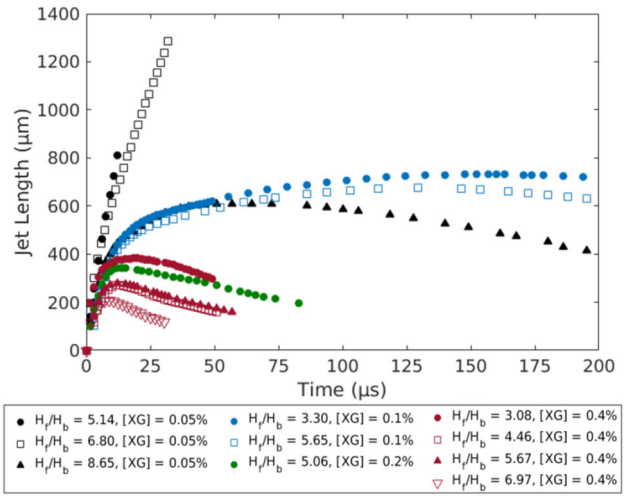

Fig. 5 Jet length versus time plot for various test cases. The fastest two cases ($H_f/H_b = 5.14$ and $H_f/H_b = 6.80$ for [XG] = 0.05 wt%) result with pinch-off, while others represent cases where jets retract back to the ink surface

Table 2 Threshold H_f/H_b values for breakup evaluated for different XG concentrations

[XG] (%)	τ_y	H_f/H_b
0.05	0.269	6.83
0.1	0.365	2.48
0.2	1.122	2.18
0.4	2.14	0.53

4 Conclusions

In summary, this work presents new insights into the mechanisms of laser-induced ejections of non-Newtonian fluids. We demonstrated that relative to Newtonian fluids with comparable surface tension, density, and viscosity, the jets induced from viscoelastic inks can stretch significantly further before breakup, whereby the amount of stretching depends on the elasticity and the relative thickness H_f/H_b of the ink layer. A threshold laser energy at which the viscoelastic fluid can stretch to the point of breakup is found, and this laser energy depends on the yield stress of the fluid. Although the experimental setup used in this study is based on BA-LIFT, the results and interpretations can apply to other LIFT techniques.

Acknowledgements We acknowledge support of the National Science Foundation (NSF) through a Materials Research Science and Engineering Center program through the Princeton Center for Complex Materials (DMR-1420541).

References

1. C.B. Arnold, P. Serra, A. Piqué, MRS Bull. **32**(01), 23 (2007)
2. A. Palla-Papavlu, V. Dinca, C. Luculescu, J. Shaw-Stewart, M. Nagel, T. Lippert, M. Dinescu, J. Opt. **12**(12), 124014 (2010)
3. B. Hopp, T. Smausz, N. Kresz, N. Barna, Z. Bor, L. Kolozsvári, D.B. Chrisey, A. Szabó, A. Nógrádi, Tissue Eng. **11**(11–12), 1817 (2005)
4. C. Boutopoulos, I. Kalpyris, E. Serpetzoglou, I. Zergioti, Microfluid. Nanofluid. **16**(3), 493 (2014)
5. A.I. Kuznetsov, C. Unger, J. Koch, B.N. Chichkov, Appl. Phys. A **106**(3), 479 (2012)
6. A. Palla-Papavlu, M. Dinescu, A. Wokaun, T. Lippert, Appl. Phys. A **117**(1), 371 (2014)
7. Z. Zhang, R. Xiong, R. Mei, Y. Huang, D.B. Chrisey, Langmuir **31**(23), 6447 (2015)
8. N.T. Kattamis, P.E. Purnick, R. Weiss, C.B. Arnold, Appl. Phys. Lett. **91**(17), 171120 (2007)

9. N.T. Kattamis, N.D. McDaniel, S. Bernhard, C.B. Arnold, Organ. Electron. **12**(7), 1152 (2011)
10. M.S. Brown, N.T. Kattamis, C.B. Arnold, J. Appl. Phys. **107**(8), 083103 (2010)
11. N.T. Kattamis, M.S. Brown, C.B. Arnold, J. Mater. Res. **26**(18), 2438 (2011)
12. M.S. Brown, N.T. Kattamis, C.B. Arnold, Microfluid. Nanofluid. **11**(2), 199 (2011)
13. M.S. Brown, C.F. Brasz, Y. Ventikos, C.B. Arnold, J. Fluid Mech. **709**, 341 (2012)
14. C.F. Brasz, C.B. Arnold, H.A. Stone, J.R. Lister, J. Fluid Mech. **767**, 811 (2015)
15. M. Duocastella, J. Fernández-Pradas, P. Serra, J. Morenza, Appl. Phys. A **93**(2), 453 (2008)
16. V. Dinca, A. Patrascioiu, J. Fernández-Pradas, J. Morenza, P. Serra, Appl. Surf. Sci. **258**(23), 9379 (2012)
17. A. Ardekani, V. Sharma, G. McKinley, J. Fluid Mech. **665**, 46 (2010)
18. M. Zirnsak, D. Boger, V. Tirtaatmadja, J. Rheol. **43**(3), 627 (1999)
19. B. Keshavarz, E.C. Houze, J.R. Moore, M.R. Koerner, G.H. McKinley, Phys. Rev. Lett. **117**(15), 154502 (2016)
20. J. Hinze, AIChE J. **1**(3), 289 (1955)